bottom 96-well culture plate containing 100 μL reaction mixture, and incubated for 30 min at room temperature. Formazan absorbance—an index of the number of lysed cells—was measured by a microplate reader at 500 nm (Viento XS, DS Pharma Biomedical, Osaka, Japan).

3.8. Apoptosis by Flow Cytometry (FCM)

A549 cells (1.0×10^6 cells) were cultured on 100-mm culture dishes, and treated with 0, 1, 10 or 100 μg/mL MgNPs-Fe_3O_4 for 24 h at 37 °C. Cells were harvested, washed gently with PBS, collected by centrifugation, and then stained using an Annexin V-FITC Kit (Beckman Coulter, Marseille, France) following the manufacturer's instructions. Cells were stained with Annexin V and propidium iodide (PI, Sigma-Aldrich, St. Louis, MO, USA), and analyzed by flow cytometry (Becton Dickinson, Franklin Lakes, NJ, USA) within 1 h of staining using the FL1 (FITC) and FL3 (PI) lines.

3.9. Measurement of Intracellular Reactive Oxygen Species (ROS)

ROS were measured using the CM-H_2DCFDA assay (Invitrogen, Carlsbad, CA, USA) according to the manufacturer's instructions. Cells (1.0×10^4 cells/well) in 24 well-plates were treated with 0, 1, 10 or 100 μg/mL MGNPs-Fe_3O_4 for 24 h at 37 °C. A fresh stock solution of 5 mM CM-H_2DCFDA was prepared in DMSO and diluted to a final concentration of 1 μM in PBS. Cells were washed with PBS, followed by incubation with 50 μL of working solution of the fluorochrome marker CM-H_2 DCFDA for 30 min. Fluorescent images were obtained using an IX2N-FL-1 microscope (Olympus, Tokyo, Japan), and analyzed using imaging soft (Photoshop Elements 8, Adobe systems, Tokyo, Japan). The data were expressed as percentage of the unexposed control.

3.10. Intracellular Reduced Glutathione (GSH) Assay

Intracellular GSH level was determined using a GSH-Glo Glutathione assay kit (Promega, Madison, WI, USA) according to the manufacturer's instructions. Briefly, cells were seeded in 96-well plates and treated with 0, 1, 10 or 100 μg/mL MgNPs-Fe_3O_4 for 24 h at 37 °C. The cells were washed with DPBS, and the GSH-Glo reagent was added to each well for 30 min at room temperature to allow the cells to convert a luciferin derivative into luciferin. Reconstituted luciferin detection reagent was then added to each well for 15 min, and the luminescent signal was measured with a Glomax multi detection system (Promega, Madison, WI, USA).

3.11. Analysis of 8-Hydroxy-2'-Deoxyguanosine (8-OH-dG) in DNA

A549 cells were incubated with 0, 1, 10 or 100 μg/mL MGNPs-Fe_3O_4 for 72 h at 37 °C (5% CO_2). The nuclear DNA was isolated by the sodium iodide method. The 8-OH-dG levels were analyzed by HPLC-ECD methods as previously described [27]. The amount of 8-OH-dG in the DNA was determined by comparison to authentic standards, and expressed as the number of 8-OH-dG per 10^6 deoxyguanosine (dG) residues.

3.12. Oxidative Stress-Related Gene Expression Analysis

A549 cells were treated with 0, 1, 10, or 100 μg/mL MgNPs-Fe_3O_4 for 24 h at 37 °C. Total RNA was isolated using ISOGEN (Nippon Gene, Tokyo, Japan), and cDNA was produced using a mixture containing Superscript RNase H Reverse Transcriptase (Invitrogen, Carlsbad, CA, USA), oligo dT primer, and 2.5 mmol/L dNTP. Quantitative real-time PCR was conducted using the LINE GENE real-time PCR detection system (BioFlux, Tokyo, Japan) with the SYBR Premix Ex Taq Perfect Real Time Kit (Takara Bio. Inc., Otsu, Japan). The PCR reaction consisted of initial thermal activation at 95 °C for 10 s and 40 cycles. Each cycle was as follows: 95 °C for 5 s; 60 °C for 26 s. PCR producs were verified by analysis of heat-dissociation curves and amplification plots. Quantitative values were acquired from linear regression of the PCR standard curve. The primer sequences of the amplified genes are as follows [28,29]; *Heme oxygenase-1*, forward 5'-GGTGATAGAAGAGGCCAAGAC-3' and reverse 5'-GCAGAATCTTGCACTTTGTTG-3', β-*actin*, forward 5'-GGATGCAGAAGG AGATCACTG-3' and reverse 5'-CGATCCACACGGAGTACTTG-3'.

3.13. Immunostaining and Flow Cytometric Analysis for $CD44^+$ Cell Fraction

A549 cells were treated with 0, 1, 10 or 100 μg/mL MgNPs-Fe_3O_4 for 24 h at 37 °C. Cells were then labeled in a PBS solution with a mouse anti-human CD44 monoclonal antibody conjugated with fluorescein isothiocyanate (clone SFF-2, Millipore, Billerica, MA, USA) for 1 h at room temperature. A mouse IgG immunoglobulin and dye conjugate IgG was used as control for non-specific binding. Flow cytometric analysis was performed with a Guava-EasyCyte*HT using Guava Express Pro software (Millipore, Billerica, MA, USA) gating for $CD44^+$ cells. A minimum of 10,000 cells was measured per sample.

3.14. Statistical Analysis

Data are presented as the mean ± standard deviation (SD). Differences between treated and untreated control cells were determined using one-way ANOVA followed by Dunnett's test. Differences were considered statistically significant at $p < 0.05$.

4. Conclusions

MgNPs-Fe_3O_4 up to a concentration of 100 μg/mL exerted minimal effect on viability of A549 cells, despite causing a significant reduction in antioxidant capacity and an increase in oxidative damage to DNA. Increased expression of an oxidative stress-related gene was not sufficient to prevent the decrease in GSH content. The decrease in the $CD44^+$ cell fraction was consistent with the observed drop in GSH concentration and increase in 8-OH-dG level.

Acknowledgments

This research was supported in part by a Grant-in-Aid for the Global COE Program from the Ministry of Education, Culture, Sports, Science and Technology of Japan, a Grant-in-Aid for Research

on Risk of Chemical Substances from the Ministry of Health, Labour and Welfare of Japan, and a Research Grand-in-Aid from Magnetic Health Science Foundation.

Conflict of Interest

The authors report no conflict of interest. The authors are responsible for the content and writing of the paper.

References

1. Chakraborty, M.; Jain, S.; Rani, V. Nanotechnology: Emerging tool for diagnostics and therapeutics. *Appl. Biochem. Biotechnol.* **2011**, *165*, 1178–1187.
2. Ramesh, V.; Ravichandran, P.; Copeland, C.L.; Gopikrishnan, R.; Biradar, S.; Goornavar, V.; Ramesh, G.T.; Hall, J.C. Magnetite induces oxidative stress and apoptosis in lung epithelial cells. *Mol. Cell. Biochem.* **2012**, *363*, 225–234.
3. Parveen, S.; Misra, R.; Sahoo, S.K. Nanoparticles: A boon to drug delivery, therapeutics, diagnostics and imaging. *Nanomedicine* **2012**, *8*, 147–166.
4. Hilger, I.; Kaiser, W.A. Iron oxide-based nanostructures for MRI and magnetic hyperthermia. *Nanomedicine* **2012**, *7*, 1443–1459.
5. Chen, B.; Sun, Q.; Wang, X.; Gao, F.; Dai, Y.; Yin, Y.; Ding, J.; Gao, C.; Cheng, J.; Li, J.; *et al.* Reversal in multidrug resistance by magnetic nanoparticle of Fe_3O_4 loaded with adriamycin and tetrandrine in K562/A02 leukemic cells. *Int. J. Nanomed.* **2008**, *3*, 277–286.
6. Sato, A.; Itcho, N.; Ishiguro, H.; Okamoto, D.; Kawai, K.; Kasai, H.; Kurioka, D.; Uemura, H.; Kubota, Y.; Watanabe, M. Magnetic nanoparticles of Fe_3O_4 enhance docetaxel-induced prostate cancer cell death. *Int. J. Nanomed.* **2013**, in press.
7. Singh, N.; Jenkins, G.J.; Asadi, R.; Doak, S.H. Potential toxicity of superparamagnetic iron oxide nanoparticles (SPION). *Nano Rev.* **2010**, *1*, 5358.
8. Karlsson, H.L.; Cronholm, P.; Gustafsson, J.; Möller, L. Copper oxide nanoparticles are highly toxic: A comparison between metal oxide nanoparticles and carbon nanotubes. *Chem. Res. Toxicol.* **2008**, *21*, 1726–1732.
9. Kim, J.E.; Shin, J.Y.; Cho, M.H. Magnetic nanoparticles: An update of application for drug delivery and possible toxic effects. *Arch. Toxicol.* **2012**, *86*, 685–700.
10. Lewinski, N.; Colvin, V.; Drezek, R. Cytotoxicity of nanoparticles. *Small* **2008**, *4*, 26–49.
11. Klein, S.; Sommer, A.; Distel, L.V.; Neuhuber, W.; Kryschi, C. Superparamagnetic iron oxide nanoparticles as radiosensitizer via enhanced reactive oxygen species formation. *Biochem. Biophys. Res. Commun.* **2012**, *425*, 393–397.
12. Holgate, S.T. Epithelial damage and response. *Clin. Exp. Allergy.* **2000**, *1*, 37–41.
13. Kitamura, H.; Okudela, K.; Yazawa, T.; Sato, H.; Shimoyamada, H. Cancer stem cell: Implications in cancer biology and therapy with special reference to lung cancer. *Lung Cancer* **2009**, *66*, 275–281.
14. Hong, S.C.; Lee, J.H.; Kim, H.Y.; Park, J.Y.; Cho, J.; Lee, J.; Han, D.W. Subtle cytotoxicity and genotoxicity differences in superparamagnetic iron oxide nanoparticles coated with various functional groups. *Int. J. Nanomed.* **2011**, *6*, 3219–3231.

15. Wiogo, H.T.R.; Lim, M.; Bulmus, V.; Yun, J.; Amal, R. Stabilization of magnetic iron oxide nanoparticles in biological media by fetal bovine serum (FBS). *Langmuir* **2011**, *27*, 843–850.
16. Birben, E.; Sahiner, U.M.; Sackesen, C.; Erzurum, S.; Kalayci, O. Oxidative stress and antioxidant defense. *World Allergy Organ J.* **2012**, *5*, 9–19.
17. Tulis, D.A.; Durante, W.; Liu, X.; Evans, A.; Peyton, K.J.; Schafer, A.I. Adenovirus-mediated heme oxygenase-1 gene delivery inhibits injury-induced vascular neointima formation. *Circulation* **2001**, *104*, 2710–2715.
18. Morita, T. Heme oxygenase and atherosclerosis. *Thromb. Vasc. Biol.* **2005**, *25*, 1786–1795.
19. Durante, W. Heme oxygenase-1 in growth control and its clinical application to vascular disease. *J. Cell Physiol.* **2003**, *195*, 373–382.
20. Park, E.J.; Yi, J.; Chung, K.H.; Ryu, D.Y.; Choi, J.; Park, K. Oxidative stress and apoptosis induced by titanium dioxide nanoparticles in cultured BEAS-2B cells. *Toxicol. Lett.* **2008**, *180*, 222–229.
21. Napierska, D.; Rabolli, V.; Thomassen, L.C.J.; Dinsdale, D.; Princen, C.; Gonzalez, L.; Poels, K.L.C.; Kirsch-Volders, M.; Lison, D.; Martens, J.A.; *et al.* Oxidative stress induced by pure and iron-doped amorphous silica nanoparticles in subtoxic conditions. *Chem. Res. Toxicol.* **2012**, *25*, 828–837.
22. Yasuda, M.; Nakano, K.; Yasumoto, K.; Tanaka, Y. CD44: Functional relevance to inflammation and malignancy. *Histol. Histopathol.* **2002**, *17*, 945–950.
23. Leir, S.H.; Baker, J.E.; Holgate, S.T.; Lackie, P.M. Increased CD44 expression in human bronchial epithelial repair after damage or plating at low cell densities. *Am. J. Physiol. Lung Cell Mol. Physiol.* **2000**, *278*, L1129–L1137.
24. Leung, E.L.; Fiscus, R.R.; Tung, J.W.; Tin, V.P.; Cheng, L.C.; Sihoe, A.D.; Fink, L.M.; Ma, Y.; Wong, M.P. Non-small cell lung cancer cells expressing CD44 are enriched for stem cell-like properties. *PLoS One* **2010**, *5*, e14062.
25. Nagano, O.; Okazaki, S.; Saya, H. Redox regulation in stem-like cancer cells by CD44 variant isoforms. *Oncogene* **2013**, in press.
26. Zhao, H.; Tanaka, T.; Mitlitski, V.; Heeter, J, Balazs, E.A.; Darzynkiewicz, Z. Protective effect of hyaluronate on oxidative DNA damage in WI-38 and A549 cells. *Int. J. Oncol.* **2008**, *32*, 1159–1167.
27. Kawai, K.; Li, Y.S.; Kasai, H. Accurate measurement of 8-OH-dG and 8-OH-Gua in mouse DNA, urine and serum: Effects of X-ray irradiation. *Genes Environ.* **2007**, *29*, 107–114.
28. Miyake, M.; Fujimoto, K.; Anai, S.; Ohnishi, S.; Kuwada, M.; Nakai, Y.; Inoue, T.; Matsumura, Y.; Tomioka, A.; Ikeda, T.; *et al.* Heme oxygenase-1 promotes angiogenesis in urothelial carcinoma of the urinary bladder. *Oncol. Rep.* **2011**, *25*, 653–660.
29. Wang, C.; Tian, Y.; Lei, B.; Xiao, X.; Ye, Z.; Li, F.; Kijlstra, A.; Yang, P. Decreased IL-27 expression in assiciation with an increased Th17 response in Vogt-Koyanagi-Harada disease. *Invest. Ophthalmol. Vis. Sci.* **2012**, *53*, 4668–4675.

J Nanopart Res (2013) 15:1653
DOI 10.1007/s11051-013-1653-y

RESEARCH PAPER

Transfection efficiency influenced by aggregation of DNA/polyethylenimine max/magnetic nanoparticle complexes

Satoshi Ota · Yoshiyuki Takahashi · Asahi Tomitaka · Tsutomu Yamada · Daisuke Kami · Masatoshi Watanabe · Yasushi Takemura

Received: 11 December 2012 / Accepted: 12 April 2013 / Published online: 25 April 2013

Abstract Gene delivery using magnetic nanoparticles (MNPs) is known as magnetofection and is an efficient non-viral gene delivery system. γ-Fe_2O_3 nanoparticles (primary diameter = 29 nm) and Fe_3O_4 nanoparticles (primary diameter = 20–30 nm) coated with deacylated linear polyethylenimine (PEI max) were prepared and conjugated with DNA. The dependency of transfection efficiency on the weight of MNPs, viability of HeLa cells, and size of DNA/PEI max/MNP complexes was evaluated. Transfection efficiency initially increased with the weight of the complexes; however, it decreased with further increase in weight. In contrast, cell viability increased with further increase in weight. Cytotoxicity assay showed that the decline in transfection efficiency at higher weights was not attributable to cytotoxicity of DNA/PEI max/MNP complexes. The DNA/PEI max/MNP complexes aggregated because of DNA binding and pH interaction with the medium. Aggregation depending on the weight of MNPs was confirmed. The number of complexes was estimated from the size distribution. In addition, the dependency of the transfection efficiency on aggregation was assessed with respect to cellular endocytic pathways using the complexes. The complexes were internalized through clathrin-dependent endocytosis, which was a size-dependent pathway. This study reveals that decreased transfection efficiency was associated with the extent of aggregation, which was induced by high weight of MNPs.

Keywords Magnetofection · Magnetic nanoparticles · Aggregation · Cytotoxicity · Endocytosis

S. Ota (✉) · Y. Takahashi · T. Yamada · M. Watanabe · Y. Takemura
Faculty of Engineering, Yokohama National University, Yokohama 240-8501, Japan
e-mail: ota-satoshi-gw@ynu.ac.jp

A. Tomitaka
Department of Materials Science and Engineering, University of Washington, Seattle, WA 98195, USA

D. Kami
Department of Cardiac Supports, Kyoto Prefectural University of Medicine, Kyoto 602-8566, Japan

Introduction

Recently, magnetic nanoparticles (MNPs) have attracted considerable attention as transfection vectors. Non-viral transfection vectors such as cationic polymers and cationic liposomes are more biocompatible than viral vectors; however, their transfection efficiency is lower (De Smedt et al. 2000; Guo et al. 2007). MNPs guide DNA into the target tissue and transfect targeted cells rapidly, and the application of magnetic fields leads to the translocation of MNPs inside the cells (Scherer et al. 2002). Coupling non-viral transfection vectors with iron oxide nanoparticles

such as polyethylenimine (PEI) (Scherer et al. 2002), polyamidoamine dendrimer (Pan et al. 2007), and PEI/poly(ethylene glycol)/chitosan copolymer (Kievit et al. 2009)–coated iron oxide nanoparticles facilitate high transfection efficiency and biocompatibility. Furthermore, surface-modified silica (Roy et al. 2005) and gold (Ghosh et al. 2008) nanoparticles have been used instead of iron oxide nanoparticles for gene delivery vectors.

PEI has a cationic charge owing to protonation of the amino nitrogen under physiological conditions (Boussif et al. 1995). PEI conjugates with DNA through electrostatic forces because PEI is cationic and DNA is anionic (Kircheis et al. 2001; Oku et al. 2001). PEI is known as both a coating and a transfection reagent (Boussif et al. 1995; Seino et al. 2009). First, MNPs tend to aggregate because of van der Waals interactions, whereas coating with PEI prevents aggregation via electrostatic repulsion (Seino et al. 2009). Second, DNA/PEI/MNP complexes are guided to cell surfaces by cationic–anionic interactions between PEI and the cell membrane (Payne et al. 2007). Third, the complexes are internalized into the cells by endocytosis promoted by ligand/receptor interactions between PEI and cell surface receptors (Godbey et al. 1999; Scherer et al. 2002). During endocytosis, the complexes are engulfed by cell membrane invaginations and encapsulated into membrane-bound vesicles known as endosomes (Sahay et al. 2010). PEI elicits proton sponge effects characterized by proton accumulation followed by passive chloride influx into endosomes. This influx causes osmotic swelling leading to endosome disruption thereby protecting DNA contained in the complexes from lysosomal degradation (Kichler et al. 2001; Akincl et al. 2005). PEI takes two forms: linear and branched. Linear PEI is less toxic compared with branched PEI (Jeong et al. 2001). In this study, PEI max, which is a deacylated linear PEI, was coated on MNPs. These MNPs were used as transfection vectors. Linear PEI contains residual *N*-acyl groups that hinder gene transfection (Thomas et al. 2005). Deacylation of linear PEI promotes transfection.

With respect to magnetofection, transfection efficiency is determined primarily by magnetic force on the particles, particle configuration in the medium, and endocytic pathway, depending on the size of particles. Magnetic force depends on magnetization, volume, magnetic permeability of MNPs (Pankfurst et al. 2003; Furlani and Xue 2012), and magnetic field gradient (Pankfurst et al. 2003; Akiyama et al. 2010; Furlani and Xue 2012). Configuration of nanoparticles in the medium is influenced by pH, concentration of particles, surface-coating agents, and serum protein (Steitz et al. 2007; Wang et al. 2009; Wigo et al. 2012). The influences of nanoparticle size on endocytosis have been investigated with poly (D, L-lactide-co-glycolide) nanoparticles fractionated to small- (<100 nm) and large-size (>100 nm) nanoparticles (Prabha et al. 2002), gold nanoparticles of size 45, 70, and 110 nm (Wang et al. 2010), and latex fluorescent beads of defined size (50–1000 nm) (Rejman et al. 2004). These studies show that high rate of cellular internalization is achieved with smaller-sized nanoparticles.

The dependency of transfection efficiency on the weight of MNPs was evaluated by determining the cytotoxicity and size of DNA/PEI max/MNPs complexes in HeLa cells. The effect of the size of the complexes on endocytic pathways was also assessed to confirm the influence of size on transfection efficiency. The novelty of this study lies in the confirmation of the MNP weight response of transfection efficiency in terms of cytotoxicity, aggregation of complexes, and endocytic pathway. Moreover, relationships between transfection efficiency and aggregation are confirmed for both γ-Fe_2O_3 and Fe_3O_4 nanoparticles.

Materials and methods

Materials and surface coating

γ-Fe_2O_3 nanoparticles (primary diameter = 29 nm) and Fe_3O_4 nanoparticles (primary diameter = 20–30 nm) were purchased from CIK NanoTek and Nanostructured & Amorphous Materials, Inc. These nanoparticles were coated with PEI max (mw 40,000) purchased from Nacalai Tesque and Polysciences, Inc.

γ-Fe_2O_3 nanoparticles (200 mg) were dispersed in 10 ml solution of 1.0 mg/ml PEI max by supersonification for 10 min. This solution was purified by centrifugation at $743\times g$ (R = 7.39 cm) for 15 min. The supernatant was centrifuged at $10{,}000\times g$ (R = 8.8 cm) for 30 min. The precipitate was collected as PEI max-coated γ-Fe_2O_3 nanoparticles (Kami et al. 2011a). For Fe_3O_4 nanoparticles,

200 mg of nanoparticles were dispersed in 40 ml solution of 1.0 mg/ml PEI max. The rest of the process was the same as for γ-Fe_2O_3 nanoparticles.

Transfection and preparation of MNP of different densities

HeLa cells from a human cervical carcinoma line were cultured in Dulbecco's modified Eagle medium (DMEM) supplemented with 10 % fetal bovine serum (FBS) and 1 % penicillin–streptomycin (PS). The cells were seeded in 35 mm dishes at a density of 200,000 cells/well on the day prior to transfection. The cells were incubated at 37 °C in a humidified atmosphere containing 5 % CO_2.

To evaluate the dependency of transfection efficiency on the weight of MNPs, solutions of 1 mg/ml PEI max and various densities of PEI max-coated MNPs were prepared. PEI max and PEI max-coated MNPs solutions (7.5 μl) were mixed with 2.5 μg of plasmid DNA expressing enhanced green fluorescent protein (EGFP) in sterile water for 15 min. DNA/PEI max complexes and DNA/PEI max/MNP complexes were added to 1 ml medium. Each medium containing DNA/PEI max complexes or DNA/PEI max/MNP complexes was added to the cells in each sample dish after removing the medium and washing the cells with phosphate-buffered saline (PBS). The weights of PEI max-coated MNPs in each 7.5 μl sample of 1 mg/ml PEI max solution were 0.75, 1.5, 2.25, 3.0, 4.5, and 7.5 μg for both γ-Fe_2O_3 and Fe_3O_4. The amount of plasmid DNA was 2.5 μg for all the samples.

Each dish containing DNA/PEI max/MNP complexes was placed on a neodymium (NdFeB) permanent magnet (diameter = 40 mm, height = 20 mm) purchased from Sangyo Supply Co. for 1 h. Each dish containing DNA/PEI max/MNP complexes was excited using a magnetic field gradient perpendicular to the dish at 26.5–33.0 T/m in the area of the dish near the cell surface. Two days after transfection, its efficiency was evaluated by fluorescence microscopy. The areas of fluorescent cells in fluorescence micrographs were compared with those of all cells observed in phase-contrast micrographs. The ratio of area of the fluorescent cells was calculated. Nine datasets were prepared for each condition of the fluorescence micrographs (three dishes prepared for each condition and three sites observed in each dish).

Cytotoxicity assay

HeLa cells were seeded in 35 mm dishes at a density of 200,000 cells/well. One day after the incubation, PEI max, PEI max-coated MNPs, DNA, DNA/PEI max complexes, and DNA/PEI max/MNP complexes were added to each dish. The method of transfection and preparation of each MNP density was the same as that for the transfection experiment. Two days after incubation, cell viability was evaluated by trypan blue dye exclusion test.

Size measurement

The hydrodynamic sizes of the PEI max-coated γ-Fe_2O_3 and Fe_3O_4 nanoparticles were measured by dynamic light scattering (DLS) method using a fiber-optical particle analyzer (FPAR-1000, Otsuka Electronics). The morphologies of the PEI max-coated γ-Fe_2O_3 nanoparticles and DNA/PEI max/γ-Fe_2O_3 nanoparticle complexes were characterized by transmission electron microscopy (TEM).

Endocytic inhibitors

Chlorpromazine and genistein were used as endocytic inhibitors. Chlorpromazine (Nacalai Tesque) inhibits clathrin-dependent endocytosis (CDE), and genistein (Nacalai Tesque and Fujicco Co.) inhibits clathrin-independent endocytosis (CIE).

In the transfection experiment, HeLa cells (200,000 cells/well) were seeded in 35 mm dishes on the day prior to the initiation of the inhibition study. The cells were preincubated with endocytic inhibitors (10 μg/ml chlorpromazine or 200 μM genistein) in 1 ml/well of medium for 30 min. Endocytic inhibitors were also added during magnetofection and incubated for 1 h after magnetofection. Chlorpromazine was diluted in sterile water, and genistein was diluted in dimethyl sulfoxide (DMSO) so that the final concentration of DMSO in the medium was <0.1 % (Gruenstein et al. 1975; Rejman et al. 2005; Vercauteren et al. 2011).

Results and discussion

Dependency of transfection efficiency on weight of MNPs and cytotoxicity assay

Figure 1 illustrates the dependency of transfection efficiency on the weight of γ-Fe_2O_3 and Fe_3O_4 nanoparticles. Transfection efficiency increased with weight, but decreased with further increases in γ-Fe_2O_3 and Fe_3O_4 (>1.5 μg). This dependency has been reported elsewhere (Plank et al. 2003; Kami et al. 2011a). For the weight of 1.5 and 2.25 μg (γ-Fe_2O_3) and 1.5, 2.25, and 3.0 μg (Fe_3O_4), differences in transfection efficiency were not significant ($p \geq 0.05$). The transfection efficiency of γ-Fe_2O_3 nanoparticles was higher compared with that of Fe_3O_4 nanoparticles at 0.75, 1.5, and 2.25 μg ($p < 0.05$). Figure 2 is fluorescent micrographic images of γ-Fe_2O_3. These images also indicated the trend of transfection efficiency shown in Figs. 1 (2).

Figure 3 illustrates the viability of HeLa cells exposed to PEI max, PEI max-coated γ-Fe_2O_3 nanoparticles, DNA, DNA/PEI max complexes, and DNA/PEI max/γ-Fe_2O_3 nanoparticle complexes. The weight of MNPs was 2.25 μg (Fig. 3). The reduction in cell viability in cells exposed to PEI max and DNA compared with the control sample without PEI max, MNPs, or DNA was negligible ($p \geq 0.05$). The cell viability of the sample with PEI max-coated MNPs, DNA/PEI max complexes, and DNA/PEI max/MNP complexes decreased in contrast to the sample with only PEI max ($p < 0.05$). In addition, viability decreased significantly in the sample with DNA/PEI/max MNP complexes in comparison with the sample containing only DNA ($p < 0.05$). Figure 4 illustrates the dependency of cell viability on the weight of MNPs. Cell viability initially decreased with weight of MNPs; however, it increased with further increase in MNP weight (above 2.25 μg; $p < 0.05$).

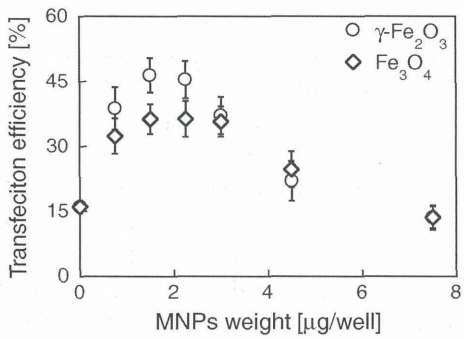

Fig. 1 Transfection efficiency as a function of magnetic nanoparticles (MNP) weight. Transfection efficiency was evaluated by fluorescent microscopy. MNP weight of 0 μg/well indicates the sample containing DNA/polyethylenimine (PEI) max complexes

Decline in transfection efficiency has been attributed to cytotoxicity of DNA/MNPs (Plank et al. 2003). However, Figs. 1 and 4 show that cell viability in contrast to the decline in transfection efficiency, increased at higher MNP weights. In addition, the γ-Fe_2O_3 nanoparticle without coating has been reported to be of low cytotoxicity (Lee et al. 2011). It has been also reported that linear PEI has low cytotoxicity at lower concentrations, but is cytotoxic at higher concentrations (Banerjee et al. 2006; Jeong et al. 2001). In this study, the cytotoxicity of HeLa cells that were exposed to PEI max was significantly low because PEI max was used in low concentrations. Decline in cell viability in PEI max-coated γ-Fe_2O_3 nanoparticles is induced by reactive oxygen species due to the formation of free hydroxyl radical species, reacting with a range of intracellular constituents, due to high internalization of γ-Fe_2O_3 nanoparticles (McCord 1998; van der Bos et al. 2003; Arsianti et al. 2010b). However, this decline was minor because of the low doses of MNP incorporated into cells. Figures 3 and 4 suggest that the cytotoxicity may be attributed to high internalization of DNA/PEI max/MNP complexes into cells. The toxicity of DNA per se was negligible (Fig. 3). Internalization of DNA/PEI max/MNP complexes decreases cell viability, probably because of the disruption of cell membrane integrity after internalization (Prijic et al. 2012). The viability of HeLa cells exposed to complexes that contained γ-Fe_2O_3 nanoparticles of 2.25 μg was reduced despite the low cytotoxicity of PEI max-coated γ-Fe_2O_3 nanoparticles. The sample with MNPs of 2.25 μg induced higher transfection efficiency. This result suggests that cytotoxicity was because of higher internalization of DNA/PEI max/MNP complexes, and the trade-off between transfection efficiency and cytotoxicity is indicated (Arsianti et al. 2010b). The dependency of transfection efficiency and cell viability on the weight of MNPs indicates that transfection efficiency was not reduced because of cytotoxicity.

Aggregation of PEI max-coated MNPs

Figure 5 illustrates the size distribution of PEI max-coated γ-Fe_2O_3 and Fe_3O_4 nanoparticles in sterile

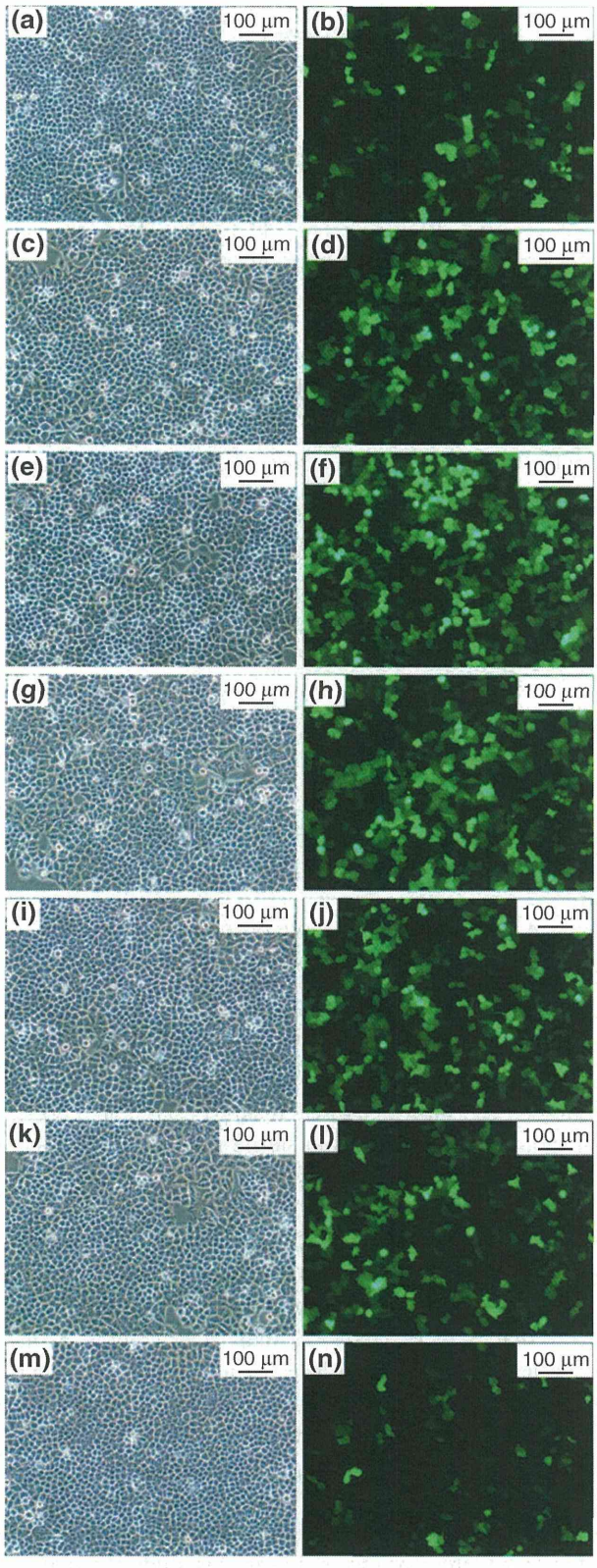

Fig. 2 Phase contrast (**a**, **c**, **e**, **g**, **i**, **k**, and **m**) and fluorescent (**b**, **d**, **f**, **h**, **j**, **l**, and **n**) micrographic images of transfected cells in the sample with γ-Fe_2O_3 of **a**, **b** 0, **c**, **d** 0.75, **e**, **f** 1.5, **g**, **h** 2.25, **i**, **j** 3.0, **k**, **l** 4.5, and **m**, **n** 7.5 μg. MNP weight of 0 μg/well indicates the sample containing DNA/polyethylenimine (PEI) max complexes

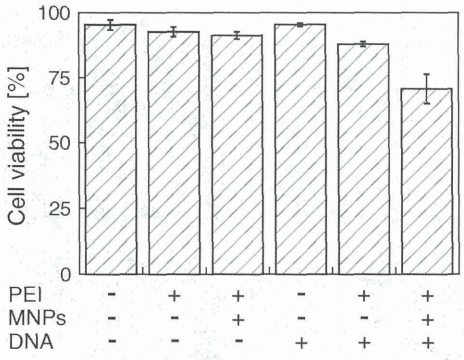

Fig. 3 Cell viability of HeLa cells in the presence of polyethylenimine (PEI) max, PEI max-coated γ-Fe_2O_3 nanoparticles, DNA, DNA/PEI max complexes, and DNA/PEI max/γ-Fe_2O_3 nanoparticle complexes. The weight of magnetic nanoparticles (MNPs) was 2.25 μg. The viability was evaluated by trypan blue dye exclusion test

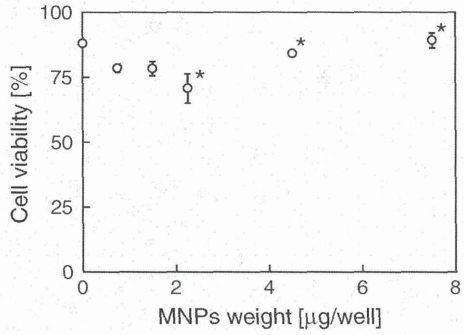

Fig. 4 Cell viability of HeLa cells as a function of the weight of polyethylenimine (PEI) max-coated γ-Fe_2O_3 nanoparticles. Magnetic nanoparticles (MNP) weight of 0 μg/well indicates the sample containing DNA/PEI max complexes. Confirmation of the dependency of cell viability on the weight of MNPs is marked with *asterisk* ($p < 0.05$)

water (Fig. 5a), DNA/PEI max/γ-Fe_2O_3 and Fe_3O_4 nanoparticle complexes in sterile water (Fig. 5b), the complexes in the medium (Fig. 5c) and pure medium, DMEM supplemented with 10 % FBS and 1 % PS (Fig. 5d) as measured by DLS. The diameters of PEI max-coated nanoparticles in sterile water were 84 ± 31 nm (γ-Fe_2O_3) and 115 ± 35 nm (Fe_3O_4). The diameters of DNA/PEI max/MNP complexes in sterile water were 126 ± 27 nm (γ-Fe_2O_3) and 116 ± 26 nm (Fe_3O_4). The diameters of the complexes in the medium were 191 ± 39 nm (γ-Fe_2O_3) and 200 ± 43 nm (Fe_3O_4). The size of the pure medium was 111 ± 27 nm. These complexes included micro-size complexes, but this finding was not considered for evaluation in this study. In sterile

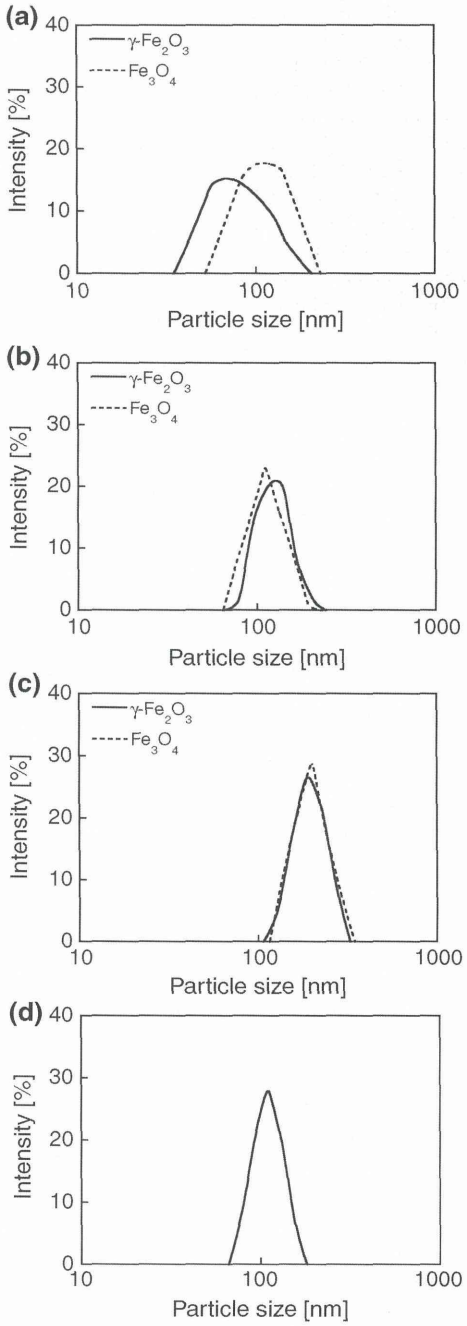

water, the size of PEI max-coated Fe_3O_4 nanoparticles is larger than that of PEI max-coated γ-Fe_2O_3 nanoparticles because the surface charge of bare Fe_3O_4 nanoparticles is lower than that of bare γ-Fe_2O_3 nanoparticles in the surface-coating process. In sterile water, bare Fe_3O_4 nanoparticles aggregate more readily than bare γ-Fe_2O_3 nanoparticles because the isoelectric point of Fe_3O_4 is nearer to the pH of sterile

◀**Fig. 5** Size distribution of **a** polyethylenimine (PEI) max-coated γ-Fe_2O_3 and Fe_3O_4 nanoparticles in sterile water, **b** DNA/PEI max/γ-Fe_2O_3 and Fe_3O_4 nanoparticle complexes in sterile water, **c** DNA/PEI max/γ-Fe_2O_3 and Fe_3O_4 nanoparticle complexes in medium, and **d** pure medium (Dulbecco's modified Eagle medium supplemented with 10 % FBS and 1 % PS) as measured by dynamic light scattering (DLS). **b** and **c** were compared in the same condition as the ratio of DNA, PEI max, and magnetic nanoparticles (MNPs) to each other. The sizes were **a** 84 ± 31 nm (γ-Fe_2O_3), 115 ± 35 nm (Fe_3O_4), **b** 126 ± 27 nm (γ-Fe_2O_3), 116 ± 26 nm (Fe_3O_4), **c** 191 ± 39 nm (γ-Fe_2O_3), 200 ± 43 nm (Fe_3O_4), and **d** 111 ± 21 nm. The complexes contained particles of micro-size, but this finding was not considered for evaluation in this study

water (pH 7.0) than that of γ-Fe_2O_3. Aggregation of PEI max-coated γ-Fe_2O_3 nanoparticles induced by DNA binding was confirmed (Fig. 5a, b). PEI max-coated Fe_3O_4 nanoparticles also aggregated because the complexes (both γ-Fe_2O_3 and Fe_3O_4) were of microsize (data not shown). PEI max-coated MNPs aggregate because of DNA binding. TEM observations also show that PEI max-coated MNPs aggregate because of conjugation with DNA (Fig. 6). Moreover, the medium induces additional aggregation of the complexes (Fig. 5b, c). The pH of culture medium is 7.4 (mildly alkaline), whereas that of sterile water is 7.0 (neutral). The positive surface charge of PEI-coated MNPs decreases owing to the mildly alkaline pH of the solvent. The complexes conjugate with serum protein contained in the medium. However, it has been reported that serum protein prevents the aggregation of MNPs modified with polymers (Wigo et al. 2012). The aggregation of the complexes in this study was reduced compared with serum-free medium because of serum proteins (data not shown).

A decrease in electrostatic repulsion due to DNA binding and mildly alkaline pH in the medium (pH 7.4) has been reported to induce aggregation of complexes (Arsianti et al. 2010a; Kami et al. 2011b; Miao et al. 2013). An increase in pH to a mildly alkaline level contributed to the instability of PEI-coated MNPs (Steitz et al. 2007; Wang et al. 2009). The models of aggregation for both γ-Fe_2O_3 and Fe_3O_4 nanoparticles are very similar.

Dependency of aggregation of DNA/PEI max/MNP complexes on weight of MNPs in the medium

Figures 7 and 8 illustrate the size distribution of the DNA/PEI max/γ-Fe_2O_3 and Fe_3O_4 nanoparticle complexes in the medium for weight of each of the MNPs as measured by DLS. The diameters of the γ-Fe_2O_3 complexes were 127 ± 27, 124 ± 24, 175 ± 41, and 191 ± 39 nm for samples with weights of 0.75, 2.25, 4.5, and 7.5 μg, respectively. The diameters of the Fe_3O_4 complexes were 141 ± 30, 144 ± 30, 152 ± 30, and 200 ± 43 nm for the samples with the weight of 0.75, 2.25, 4.5, and 7.5 μg, respectively. The samples contained micro-size complexes, but this finding was not considered for evaluation in this study. The size distributions indicated that aggregation was due to high weight of MNPs, except in the samples of 0.75 and 2.25 μg as confirmed for γ-Fe_2O_3 and Fe_3O_4 complexes. This result indicates that the concentration of MNPs in the medium influences the aggregation of the complexes and that higher concentration induces higher aggregation. This aggregation affects transfection efficiency, which depends on the weight of MNPs (Fig. 1). The differences in transfection efficiency between γ-Fe_2O_3 and Fe_3O_4 are also influenced by the size of complexes. However, comparison of transfection efficiency between nanoparticles such as γ-Fe_2O_3 and Fe_3O_4 must take into account magnetization as a factor, influencing magnetic force on the particles (Johnson et al. 1975; Pankfurst et al. 2003; Furlani and Xue 2012).

In addition, the number of DNA/PEI max/MNP complexes was estimated by the following equation:

$$N = \frac{M}{VP} \tag{1}$$

where N is the number of complexes, M is the weight of MNPs used in each condition, V is the volume of complexes, and P is the bulk density of the MNPs. The volume was estimated by the following equation on the basis of the size distribution:

$$V = \sum_{k=1}^{n} \frac{4}{3}\pi\left(\frac{D_k}{2}\right)^3 F_k \tag{2}$$

where D is the diameter of the complexes, F is the fraction of the complexes of each diameter, and n is the number of measurement points. This estimate is rough because the complexes are not perfect spheres. However, this estimate gives excellent insight into the influence of MNP weight on transfection efficiency. The number of complexes decreased with increasing sizes of the complexes and the sizes

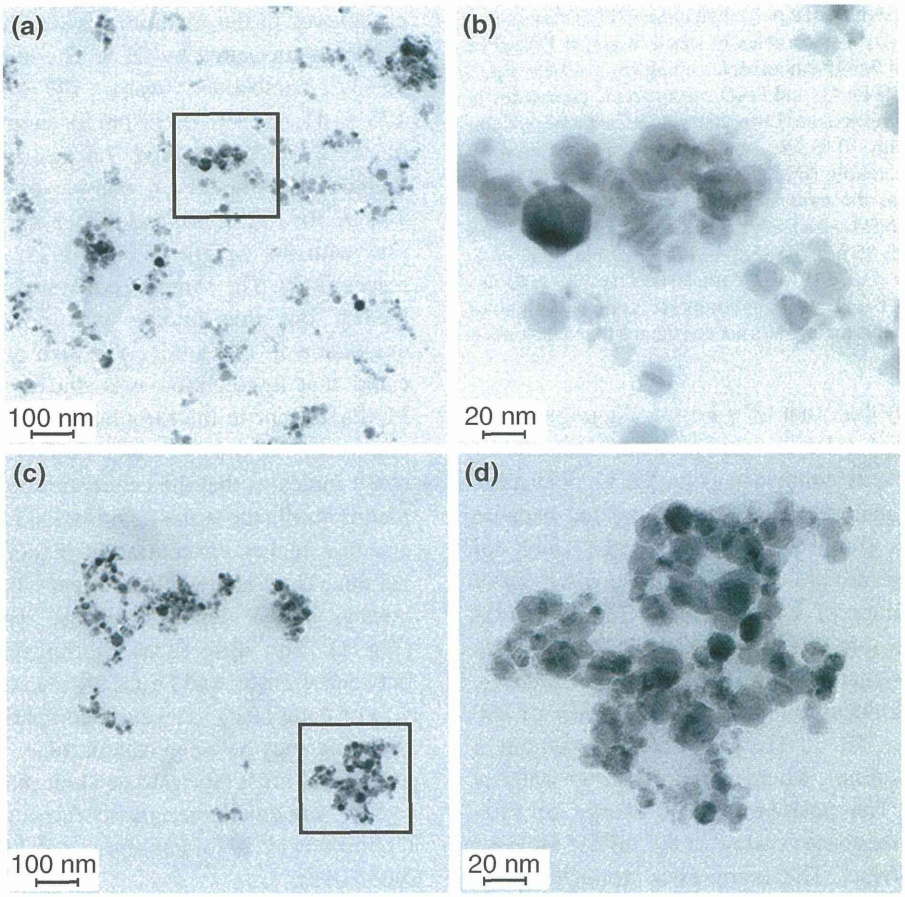

Fig. 6 Transmission electron microscopy (TEM) images of **a** polyethylenimine (PEI) max-coated magnetic nanoparticles (MNPs) (γ-Fe_2O_3 nanoparticles), **b** PEI max-coated MNPs magnified from **a**, **c** DNA/PEI max/MNP (2.25 μg/well γ-Fe_2O_3 nanoparticle) complexes, **d** DNA/PEI max/MNP complex magnified from **c**. These were observed in sterile water. These images show that the complexes were larger than the PEI max-coated MNPs

increased because of aggregation. Figure 9 illustrates that the trend of transfection efficiency is according to the number of γ-Fe_2O_3 complexes. The number of complexes of size up to 200 nm was indicated by this estimate because higher internalization is confirmed to be achieved with nanoparticles of size up to 200 nm (Rejman et al. 2004). This trend was also confirmed for Fe_3O_4 complexes (data not shown). It is possible that aggregation affects transfection efficiency because of cellular uptake inhibition and reduction in the number of complexes.

Endocytic pathways of DNA/PEI max/MNP complexes

The endocytic pathways of the DNA/PEI/MNP complexes were similar to those of PEI polyplexes (Huth et al. 2004). Endocytosis is divided into phagocytosis (the uptake of large particles) and pinocytosis (the uptake of fluids and solutes). Pinocytosis is classified into clathrin-dependent endocytosis (CDE) and clathrin-independent endocytosis (CIE) (Sahay et al. 2010). Nanoparticles with diameter up to 200 nm are internalized by CDE (Rejman et al. 2004), whereas nanoparticles that are not internalized by CDE enter the cells by CIE, for example caveolae- and flotillin-dependent endocytosis (Rejman et al. 2004; Payne et al. 2007). Flotillin-dependent endocytosis is PEI receptor (proteoglycan)-mediated pathway (Zanta et al. 1997; Zou et al. 2000), and proteoglycan is known as cell surface receptor binding cationic substrates (Mislick and Baldeschwieler 1996). Receptor-mediated endocytosis is induced by interaction between ligand and receptor bound to the cell surface.

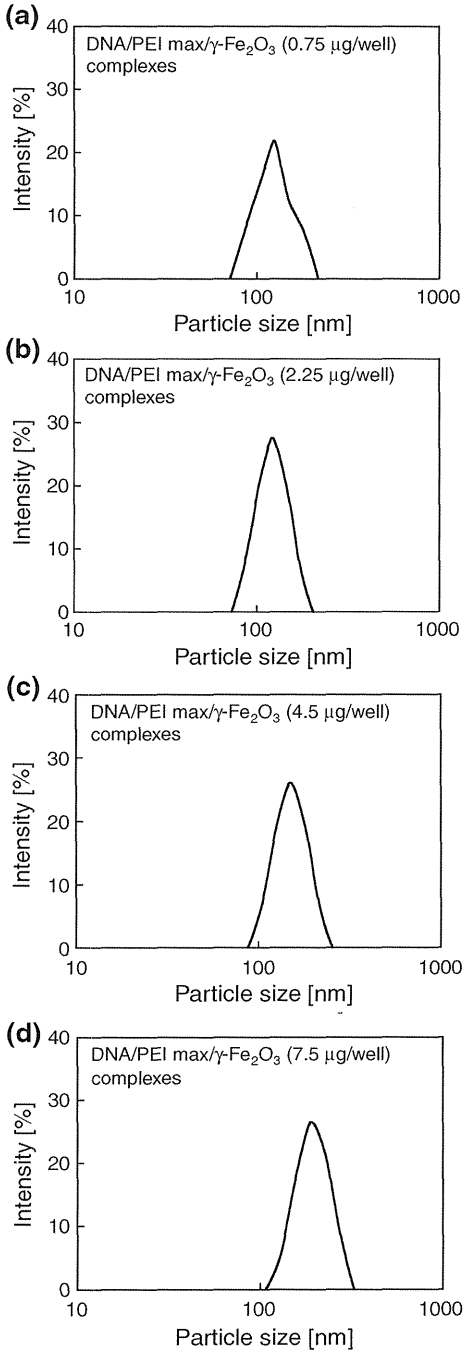

Fig. 7 Size distribution of DNA/polyethylenimine (PEI) max/γ-Fe_2O_3 nanoparticle complexes in medium, as measured by dynamic light scattering (DLS) for **a** 0.75 μg/well, **b** 2.25 μg/well, **c** 4.5 μg/well, and **d** 7.5 μg/well, and the sizes of the complexes were **a** 127 ± 27 nm, **b** 124 ± 24 nm, **c** 152 ± 30 nm, **d** 191 ± 39 nm, respectively. The samples contained micro-order size complexes, but this finding was not considered for evaluation in this study

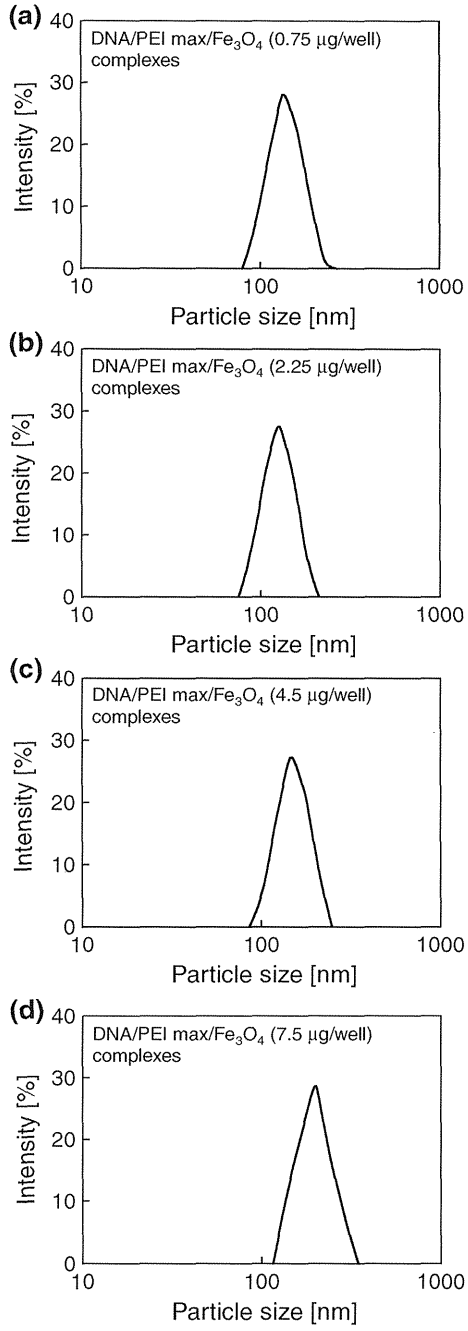

Fig. 8 The size distribution of DNA/polyethylenimine (PEI) max/Fe_3O_4 nanoparticle complexes in the medium as measured by dynamic light scattering (DLS) for **a** 0.75 μg/well, **b** 2.25 μg/well, **c** 4.5 μg/well, **d** 7.5 μg/well, and the size of the complexes were **a** 141 ± 30 nm, **b** 144 ± 30 nm, **c** 152 ± 30 nm, **d** 200 ± 43 nm, respectively. The samples contained micro-order size complexes, but this finding was not considered for evaluation in this study

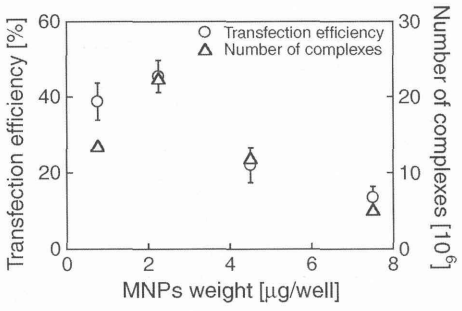

Fig. 9 The number of DNA/polyethylenimine (PEI) max/magnetic nanoparticles (MNP) complexes assessed on the basis of size distribution compared with the transfection efficiency. The trend in transfection efficiency corresponds to the numbers of complexes

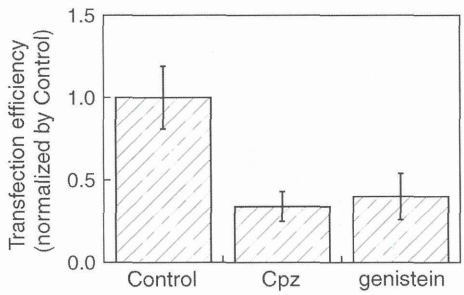

Fig. 10 Effects of inhibitors on the transfection efficiency of γ-Fe2O3 nanoparticles (control: inhibitor-free, Cpz: addition of chlorpromazine, genistein: addition of genistein). 10 μg/ml chlorpromazine or 200 μM genistein was added

With respect to receptor-mediated endocytosis, the model of endocytosis for efficient internalization has been reported (Gao et al. 2005; Decuzzi and Ferrari 2007; Lunov et al. 2011). Wrapping time, and threshold and optimal radii of particles are important factors for particle endocytosis. These factors can be represented as the function of receptor/ligand density ratio and estimated by receptor/ligand binding energy factor, bond elasticity factor, and non-specific attractive/repulsive factor at cell/particle interface (Gao et al. 2005; Decuzzi and Ferrari 2007). Moreover, wrapping time is also represented as the function of the forces acting on particle captured by receptors, which contain the elastic forces of the cellular membrane and the internal forces of receptor (Lunov et al. 2011). The optical radius of particles is estimated from wrapping time, cell lateral size, and the number of nanoparticles captured per second (Lunov et al. 2011). Optimal size of nanoparticle is up to 50 nm for efficient internalization by receptor-mediated endocytosis (Gao et al. 2005). On the other hand, in vitro test has indicated that nanoparticle with diameter up to 100–200 nm is optimal (Win and Feng 2005). Therefore, the estimation for efficient internalization must take into account the factors influenced on particle configuration, coating agent, cell type, and cultural environment.

Figure 10 illustrates the transfection rate for DNA/PEI max/MNP (γ-Fe_2O_3 of 2.25 μg) complexes in the presence of chlorpromazine as a CDE inhibitor and genistein as a CIE inhibitor. The transfection rate was decreased by both endocytic inhibitors, showing that the complexes were internalized by CDE and CIE. This result agrees with those of previous studies (Huth et al. 2004). DNA/PEI max/MNP complexes are internalized by CDE and caveolae- and flotillin-dependent endocytosis, which are classified as CIE because cellular internalization of polyplexes through these endocytic pathways has been confirmed (Huth et al. 2004; Rejman et al. 2005; Payne et al. 2007; Vercauteren et al. 2011). It is indicated that the efficient internalization of the complexes depends on the size of the complexes and other factors such as the number of complexes and the ligand/receptor interactions between PEI and PEI receptors on cell surfaces.

Conclusion

Magnetofection using DNA/PEI max/MNP complexes was studied. Transfection efficiency was enhanced using MNPs and an applied magnetic field, but it decreased with high weight of MNPs despite the increase in cell viability. DNA/PEI max/MNP complexes aggregated because of alkaline pH of the medium and the reduction in electrostatic repulsion induced by DNA binding. The sizes of the complexes increased with high weight of MNPs in the medium. Aggregation induced by high weight of MNPs inhibited cellular uptake by size-dependent endocytosis and led to a decline in the number of complexes. The decline of transfection efficiency in high weight of MNPs was due to aggregation of the complexes; therefore, it was concluded that this decline was not due to cytotoxicity.

References

Akincl A, Thomas M, Klibanov AM, Langer R (2005) Exploring polyethylenimine-mediated DNA transfection and the proton sponge hypothesis. J Gene Med 7:657–663

Akiyama H, Ito A, Kawabe Y, Kamihira M (2010) Genetically engineered angiogenic cell sheets using magnetic force-based gene delivery and tissue fabrication techniques. Biomaterials 31:1251–1259

Arsianti M, Lim M, Marquis CP, Amal R (2010a) Assembly of polyethylenimine-based magnetic iron oxide vectors: insight into gene delivery. Langmuir 26:7314–7326

Arsianti M, Lim M, Marquis CO, Amal R (2010b) Polyethylenimine based magnetic iron-oxide vector: the effect of vector component assembly on cellular entry mechanism, intracellular localization, and cellular viability. Biomacromolecules 11:2521–2531

Banerjee P, Weissleder R, Bogdanov A Jr (2006) Linear polyethylenimine grafted to a hyperbranched poly(ethylene glycol)-like core: a copolymer for gene delivery. Bioconjug Chem 17:125–131

Boussif O, Lezoualc'h F, Zanta MA, Mergny MD, Scherman D, Demeneix B, Behr J (1995) A versatile vector for gene and oligonucleotide transfer into cells in culture and in vivo: polyethylenimine. Proc Natl Acad Sci USA 92:7297–7301

De Smedt SC, Demeester J, Hennink WE (2000) Cationic polymer based gene delivery systems. Pharm Res 17: 113–126

Decuzzi P, Ferrari M (2007) The role of specific and non-specific interactions in receptor-mediated endocytosis of nanoparticles. Biomaterials 28:2915–2922

Furlani EP, Xue X (2012) Field, force and transport analysis for magnetic particle-based gene delivery. Microfluid Nanofluidics 13:589–602

Gao H, Shi W, Freund LB (2005) Mechanism of receptor-mediated endocytosis. Proc Natl Acad Sci USA 102:9469–9474

Ghosh PS, Kim C, Han G, Forbes NS, Rotello VM (2008) Efficient gene delivery vectors by tuning the surface charge density of amino acid-functionalized gold nanoparticles. ACS Nano 2:2213–2218

Godbey WT, Wu KK, Mikos AG (1999) Poly(ethylenimine) and its role in gene delivery. J Control Release 60:149–160

Gruenstein E, Rich A, Weihing RR (1975) Actin associated with membranes from 3T3 mouse fibroblast and HeLa cells. J Cell Biol 64:223–234

Guo X, Kim KS, Liu D (2007) Nonviral gene delivery: what we know and what is next. AAPS J 9:E92–E104

Huth S, Lausier J, Gersting SW, Rudolph C, Plank C, Welsch U, Rosenecker J (2004) Insight into the mechanism of magnetofection using PEI-based magnetofection for gene transfer. J Gene Med 6:923–936

Jeong JH, Song DH, Lim DW, Lee H, Park TG (2001) DNA transfection using poly(ethylenimine) prepared by controlled acid hydrolysis of poly(2-ethyl-2-oxazoline). J Control Release 73:391–399

Johnson HP, Lowrie W, Kent DV (1975) Stability of anhysteretic remanent magnetization in fine and coarse magnetite and maghemite particles. Geophys J R Astr Soc 41:1–10

Kami D, Takeda S, Makino H, Toyoda M, Gojo S, Kyo S, Umezawa A, Watanabe M (2011a) Efficient transfection method using deacylated polyethylenimine-coated magnetic nanoparticles. J Artif Organs 14:215–222

Kami D, Takeda S, Toyoda M, Watanabe M (2011b) Application of magnetic nanoparticles to biomedicine. Int J Mol Sci 11:3705–3722

Kichler A, Leborgne C, Coeytaux E, Danos O (2001) Polyethylenimine-mediated gene delivery: a mechanistic study. J Gene Med 3:135–144

Kievit FM, Veiseh O, Bhattarai N, Fang C, Gunn JW, Lee D, Ellenbogen RG, Olson JM, Zhang M (2009) PEI–PEG–chitosan copolymer coated iron oxide nanoparticles for safe gene delivery: synthesis, complexation, and transfection. Adv Funct Mater 19:2244–2251

Kircheis R, Wightman L, Wagner E (2001) Design and gene delivery activity of modified polyethylenimines. Adv Drug Deliv Rev 53:341–358

Lee KJ, An JH, Shin JS, Kim DH, Yoo HS, Cho CK (2011) Biostability of γ-Fe_2O_3 nano particles evaluated using an in vitro cytotoxicity assays on various tumor cell lines. Curr Appl Phys 11:467–471

Lunov O, Zablotskii V, Syrovets T, Röcker C, Tron K, Nienhaus GU, Simmet T (2011) Modeling receptor-mediated endocytosis of polymer-functionalized iron oxide nanoparticles by human macrophage. Biomaterials 32:547–555

McCord JM (1998) Iron free radicals, and oxidative injury. Semin Hematol 35:5–12

Miao L, Zhang K, Oiao C, Jin X, Zhang C, Yang B, Sun H (2013) Antitumor effect of human TRAIL on adenoid cystic carcinoma using magnetic nanoparticle–mediated gene expression. Nano-medicine 9:141–150

Mislick KA, Baldeschwieler JD (1996) Evidence for the role of proteoglycans in cation-mediated gene transfer. Proc Natl Acad Sci USA 93:12349–12354

Oku N, Yamazaki Y, Matsuura M, Sugiyama M, Hasegawa M, Nango M (2001) A novel non-viral gene transfer system, polycation liposomes. Adv Drug Deliv Rev 52:209–218

Pan B, Cui D, Sheng Y, Ozkan C, Gao F, He R, Li Q, Xu P, Huang T (2007) Dendrimer-modified magnetic nanoparticles enhance efficiency of gene delivery system. Cancer Res 67:8156–8163

Pankfurst QA, Connolly J, Jones SK, Dobson J (2003) Applications of magnetic nanoparticles in biomedicine. J Phys D 36:R167–R181

Payne CK, Jones SA, Chen CC, Zhuang X (2007) Internalization and trafficking of cell surface proteoglycans and proteoglycan-binding ligand. Traffic 8:389–401

Plank C, Schillinger U, Scherer F, Bergemann C, Rémy JS, Kröetz F, Anton M, Lausier J, Rosenecker J (2003) The magnetofection method: using magnetic force to enhance gene delivery. Biol Chem 384:737–747

Prabha S, Zhou WZ, Panyam J, Labhastwar V (2002) Size-dependent of nanoparticle-mediated gene transfection: studies with fractionated nanoparticles. Int J Pharm 244:105–115

Prijic S, Prosen L, Cemazar M, Scancar J, Romih R, Lavrencakv J, Bregar VB, Coer A, Krzan M, Znidarsic A, Sersa G (2012) Surface modified magnetic nanoparticles for immuno-gene therapy of murine mammary adenocarcinoma. Biomaterials 233:4379–4391

Rejman J, Oberle V, Zuhorn IS, Hoekstr D (2004) Size-dependent internalization of particles via the pathways of clathrin-and caveolae-mediated endocytosis. Biochem J 377:159–169

Rejman J, Bragonzi A, Conese M (2005) Role of clathrin- and caveolae-mediated endocytosis in gene transfer mediated by lipo- and polyplexes. Mol Ther 12:468–474

Roy I, Ohulchanskyy TY, Bharali DJ, Pudavar HE, Mistretta RA, Kaur N, Prasad PN (2005) Optical tracking of organically modified silica nanoparticles as DNA carriers: a nonviral, nanomedicine approach for gene delivery. Proc Natl Acad 102:279–284

Sahay G, Alakhova DY, Kabanov AV (2010) Endocytosis of nanomedicines. J Control Release 145:182–195

Scherer F, Anton M, Schillinger U, Henke J, Bergemann C, Krüger A, Gänsbacher B, Plank C (2002) Magnetofection: enhancing and targeting gene delivery by magnetic force in vitro and in vivo. Gene Ther 9:102–109

Seino S, Matsuoka Y, Kinoshita T, Nakagawa T, Yamamoto TA (2009) Dispersibility improvement of gold/iron-oxide composite nanoparticles by polyethylenimine modification. J Magn Magn Mater 321:1404–1407

Steitz B, Hofmann H, Kamau SW, Hassa PO, Hottiger MO, Rechenberg B, Hofmann-Amtenbrink M, Petri-Fink A (2007) Characterization of PEI-coated superparamagnetic iron oxide nanoparticles for transfection: size distribution, colloidal properties and DNA interaction. J Magn Magn Mater 311:300–305

Thomas M, Lu JJ, Ge Q, Zhang C, Chen J, Klibanov AM (2005) Full deacylation of polyethylenimine dramatically boosts its gene delivery efficiency and specificity to mouse lung. Proc Natl Acad Sci USA 102:5679–5684

van den Bos EJ, Wagner A, Mahrholdt H, Thompson RB, Morimoto Y, Sutton BS, Judd RM, Taylor DA (2003) Improved efficacy of stem cell labeling for magnetic resonance imaging studies by the use of cationic liposomes. Cell Transplant 12:743–756

Vercauteren D, Piest M, van der Aa LJ, Al Soraj M, Jones AT, Engbersen JF, De Smedt SC, Braeckmans K (2011) Flotillin-dependent endocytosis and a phagocytosis-like mechanism for cellular internalization of disulfide-based poly(amido amine)/DNA polyplexes. Biomaterials 32:3072–3084

Wang X, Zhou L, Ma Y, Li X, Gu H (2009) Control of aggregation size of polyethylenimine-coated magnetic nanoparticles for magnetofection. Nano Res 2:365–372

Wang S, Lee C, Chiou A, Wei P (2010) Size-dependent endocytosis of gold nanoparticles studied by three-dimensional mapping of plasmonic scattering images. J Nanobiotech 8:33

Wigo HTR, Lim M, Bulmus V, Gutiérrez L, Woodward RC, Amal R (2012) Insight into serum protein interactions with functionalized magnetic nanoparticles in biological media. Langmuir 28:4346–4356

Win KY, Feng S (2005) Effects of particle size and surface coating on cellular uptake of polymeric nanoparticles for oral delivery of anticancer drugs. Biomaterials 26: 2713–2722

Zanta M, Boussif O, Adib A, Behr J (1997) *In vitro* gene delivery to hepatocytes with galactosylated polyethylenimine. Bioconjug Chem 8:839–844

Zou S, Erbacher P, Remy JS, Behr J (2000) Systemic linear polyethylenimine (L-PEI)-mediated gene delivery in the mouse. J Gene Med 2:128–134